ijrr

The International Journal of Robotics Research
29(13) 1684–1704

DOI: 10.1177/0278364910364164
ijr.sagepub.com
SAGE

# Mimetic Communication Model with Compliant Physical Contact in Human–Humanoid Interaction*

**Dongheui Lee[1], Christian Ott[2] and Yoshihiko Nakamura[3]**

**Abstract**

*In this paper we aim at extending imitation learning to physical human–robot interaction (pHRI) including contact transitions (from non-contact to contact and vice versa). For interactive learning of pHRI, the paper raises four key issues: (1) motion imitation, (2) understanding motion primitives, (3) understanding interaction primitives, and (4) physical contact establishment. These issues are solved by (1) marker control, (2) mimesis model, (3) mimetic communication model, and (4) real-time motion reshaping and impedance control, respectively. The simple human motion imitation is realized by a direct marker control method in which the robot is virtually connected to the markers attached to the human via virtual springs. Learning procedures are based on ''imitation of a human'' and ''active involvement'' of the robot during the learning. The ''imitation of a human'' scheme provides efficient learning. The ''active involvement'' scheme supports incremental learning and it also enables to acquire sensory information for physical contacts. By modifying the mimetic communication model proposed by Nakamura et al., we achieve communication in physical domain as well as the symbolic domain. The communication in the symbolic domain is realized through the concept of motion primitives and interaction primitives. In the physical domain, the trajectory of the motion primitive is reshaped in accordance with the human's motions in real-time. Moreover, for performing compliant contact motion, an appropriate impedance controller is integrated into the setting. All of the presented concepts are applied to ''high five''-like interaction tasks and evaluated in experiments with a human-size humanoid robot.*

**Keywords**

Mimetic communication, physical human–robot interaction, imitation learning, marker control, impedance control

## 1. Introduction

In order to coexist with humans in the human society, robots require natural human–robot interaction (HRI) capabilities. Roughly speaking, research on HRI can be divided into cognitive HRI (cHRI) and physical HRI (pHRI). While the former focuses on the social-cognitive skills involving issues such as shared attention, initiative taking, action planning, etc., the latter copes with the actual exchange of forces and physical power. The key issues in pHRI are the realization of dexterous manipulation skills, safety and dependability, stability in contact with varying and uncertain environments, and the identification and control of varying contact states. Applications for HRI include collaborative manipulation (Kosuge and Hirata 2004), entertainment, domestic help, mental healing robots (Shibata et al. 1999), elderly care, dance partners (Kosuge and Hirata 2004), etc. Note that in most of these examples, aspects of both cHRI and pHRI are relevant.

The most basic key element of HRI is communication, which can be generalized as an exchange of symbol sequences between individuals. The media have various forms such as words, signs, images, sounds, behaviors, and so on. Mimesis theory (Donald 1991) explains that symbolic communication of the human society had developed from continuous behavioral exchange before the language skill was developed. We can now associate a symbol from a segment of behavior and vice versa. The

[1] Department of Electrical Engineering and Information Technology, Technical University of Munich, Munich, Germany
[2] Institute of Robotics and Mechatronics, German Aerospace Center (DLR), Wessling, Germany
[3] Department of Mechano-Informatics, The University of Tokyo, Tokyo, Japan

**Corresponding author:**
Christian Ott, Institute of Robotics and Mechatronics, German Aerospace Center (DLR), P.O. Box 1116, D-82234 Wessling, Germany
Email: christian.ott@dlr.de

*An earlier version of this work without physical interaction was presented at the IEEE–RAS International Conference on Humanoid Robots, 2008 (Ott et al. 2008). Results related to physical interaction were presented at the IEEE International Conference on Robotics and Automation 2009 (Lee et al. 2009).

communication through behavioral media then follows the generalized communication model of exchanging a symbol sequence. The uniqueness of communication by behavioral media lies in the physics, more precisely in the physical contacts. The behavioral communication happens in two domains, the physical domain and the symbolic domain, which both should be incorporated into a ''complete'' HRI system.

Imitation is an efficient strategy for motor learning which drastically reduces the size of the state-action space that needs to be explored (Schaal 1999). According to Donald (1991), behavioral imitation is a bidirectional process which can lead to high-level intelligence. The mirror neuron system shows this clear bidirectional process of imitation which is activating both for generation of self-motions and recognition of others' motions (Gallese et al. 1996; Rizzolatti et al. 1996). Also, their relations to the development of communication have been considered (Rizzolatti and Arbib 1998; Rizzolatti and Craighero 2004).

From the above evidence (Schaal 1999; Donald 1991; Rizzolatti and Craighero 2004), we believe that imitative learning may be a route to develop cognitive processes for motion understanding and communication in humanoid robots. Therefore, this paper introduces an imitative learning approach for motion primitive and interaction primitive learning. Among the various issues related to HRI, in brief, we aim at extending imitation learning for HRI by incorporating physical contacts. In contrast to most conventional human–robot coordination systems, we consider physical contact tasks, in which transitions between non-contact and contact states occur. These contact transitions clearly must be handled by the real-time control, but moreover must also be actively learned by the higher-level reasoning part in order to make the robot understand the cutaneous element of the HRI. In other words, the treatment of physical contact tasks involving contact transitions has implications both for the cognitive and the physical part of the interaction, and thus requires a close interplay between the involved learning and control algorithms.

In particular, we take ''high five''-like interactions, in which physical contact transitions from non-contact to contact and vice versa occur, as a benchmark task. For this type of physical interaction, the expected contact points are restricted to the robot's and human's hands. In order to learn behavioral communication in the physical world, several key issues must be addressed: motion imitation, motion learning, motion recognition, motion generation, interaction learning, interaction recognition, interaction strategy decision, and compliant motion control. The contributions of this paper are summarized by the following three components.

(1) *Imitation by marker control* (Section 3). For imitating a human motion, we design a marker control method using optical markers attached to the human demonstrator. We aim at making the robot follow the whole set of markers as good as possible, by connecting the markers with corresponding points on the humanoid by virtual springs. Our approach does not require the implementation of a computationally expensive inverse kinematics and avoids a hard priority order between the markers. This makes it suitable for tracking a rather large set of marker points (20 in the experiments).

(2) *Imitative and active learning of interaction primitives* (Section 4). On top of the marker control, frameworks for understanding motion primitives and interaction primitives are integrated so that the robot can imitate and react to human movements while understanding the meaning of the movements. Herein, the robot learns the interaction primitives by ''imitating the human'' and ''involving itself actively in the learning process''. The causality of motions (the pair of the self-action and the other's reaction) and contact information (where and when contact occurs) are trained. Once interaction primitives are learned, they are used for a high-level interaction strategy which selects an appropriate motion primitive to the partner's action.

(3) *Real-time motion adaptation for physical contact* (Section 5). Since the human user cannot be expected to reproduce his own motions always in exactly the same way, the robot has to adapt its motion according to the actual human's behavior in real-time. This is achieved by modifying the marker control based on learned expected contact information. Note that the learned primitives and the controller are tightly connected. In addition, in order to allow for ''smooth'' contact between the human and the robot, we combine the marker-based tracking control with an underlying impedance controller which allows us to realize compliant motions and to limit the contact forces.

## 2. Related Works

### *2.1. Human Motion Imitation*

Planning of whole body motions for humanoid robots is made complicated by the handling of a large number of degrees of freedom as well as by the specific constraints related to the ground reaction force (Nakamura and Yamane 2000; Kuffner et al. 2001; Kanehiro et al. 2008). The idea of using a three-dimensional motion capture system for copying a human's motion directly to a humanoid robot instead of performing complicated motion planning optimizations, therefore, has drawn the attention of many robotics researchers in the past decade (Pollard et al. 2002; Schaal et al. 2003; Nakaoka et al. 2005). In the work of Nakaoka et al. (2005), a humanoid robot performed Japanese traditional dance, which was recorded by a motion capture system. In the recent research of Demircan et al. (2008) and Dariush et al. (2008), the motion following controller was developed directly in task space, respectively marker space. In Demircan et al. (2008), a solution based on the operational space approach (Khatib 1987) was presented, such that an inverse kinematics is no longer necessary. Therein, different priorities were assigned to the markers and realized based on projections into subsequent

nullspaces. Dariush et al. (2008) utilize a mature task space kinematic control method, namely the ''closed-loop inverse kinematics'' (CLIK), in order to realize the motion tracking directly in task space. In particular, they consider full six-dimensional task descriptors from vision. However, these approaches do not deal with motion learning or HRI.

Based on the ideas of these works, our approach for the online motion imitation also aims at a control solution in task space. In contrast to Demircan et al. (2008), we avoid a hard priority order between the markers, since this would be impractical for a large marker set. Instead, we aim at making the robot follow the whole set of markers as closely as possible. Therefore, we connect the markers with corresponding points on the humanoid by virtual springs. In that way we avoid the computation of a computationally more expensive inverse kinematics via a generalized inverse of the Jacobian as was used in Dariush et al. (2008). Moreover, the springs are acting on a simulation of a simplified version of the robot dynamics. The joint angles resulting from this simulation are used to command the joint position controllers of the robot, avoiding the need for precise torque control.

## 2.2. Imitation Learning

Surveys on motion learning by imitation can be found in Schaal et al. (2003), Breazeal and Scassellati (2002), and Billard et al. (2008). Imitation learning drastically reduces the amount of trial-and-error to accomplish the movement goal by providing a successful example (Schaal 1999). The idea of symbols or motion primitives has been implemented by several mathematical frameworks. Hidden Markov models (HMMs) are used for generalization of movements demonstrated to a robot multiple times in Inamura et al. (2004), Dillmann (2004), Asfour et al. (2006), and Billard et al. (2006). HMMs allow spatiotemporal variabilities to be represented in a stochastic way. In the work of Calinon and Billard (2007), the principal component analysis (PCA) is used for dimension reduction, and the motion in the latent space is represented probabilistically through Gaussian mixture regression. Another line of research uses non-linear dynamical systems for the representation of motion primitives (Ijspeert et al. 2002; Okada et al. 2002; Peters et al. 2003). Tani and Ito (2003) describe a system for imitation learning by utilizing a recurrent neural network model with parameter biases (RNNPB), which can store and display motor behaviors. In their method, each different set of parameter biases corresponds to a motion primitive.

By involving the concepts of symbols and motion primitives, robots can not only follow human motions by simple mimicry, but also learn the motions via abstract forms and use them later for motion recognition and generation. Furthermore, adopting the abstract symbol is a good strategy for efficient computation when considering a huge search space in the real world with limited computation capabilities. Inspired by the above-mentioned works, the concept of motion primitives is used as the baseline of imitation learning in our approach. While these approaches focused on the motion primitive level and did not include interaction primitive learning, our approach extends the imitation learning to pHRI.

## 2.3. Human–Robot Interaction

Roughly speaking, HRI research can be categorized into cHRI and pHRI. In cHRI, social-cognitive skills such as joint attention and interactive learning have been studied. To build social skills for robots, Nagai et al. (2003) and Sumioka et al. (2008) focused on ''joint attention'', an important cognitive function for the emergence of communication. They proposed a computational model to explain the developmental mechanism of infant joint attention and to demonstrate that the ability of joint attention could develop without any external evaluation from a human caregiver. They addressed joint attention focusing on visual interaction and behavioral interaction by looking at a salient object. As shown in these works, robots often use body motions, because communication through motion patterns is one of the basic elements for interaction including social skills. In that sense, learning body motions and behavioral communication is closely connected to cHRI.

In the robot control society, pHRI is often studied from the viewpoint of safety and dependability (Santis et al. 2008). In particular, there has recently been great interest in the role of active and passive compliance in robot actuation (Bicchi and Tonietti 2004; Zinn et al. 2004; Albu-Schäffer et al. 2008). Passive compliance and lightweight design for protecting the robot and the human during collision seem crucial especially when considering a contact at a very high-frequency domain, i.e. for rigid impacts (Albu-Schäffer 2008), but require specialized hardware. Considering cooperative interaction between robots and humans, the (expected) physical interaction often happens at a slower frequency domain, in which also active compliance methods can be useful for limiting the contact forces. Impedance control (Hogan 1985) is one prominent example of a compliant motion control approach which allows the risk for human users interacting with the robot to be reduced by giving the robot a compliant behavior via control. Our strategy in this paper aims at giving the robot locally a certain stiffness behavior which is sufficiently compliant to perform rather slow ''high five''-like contact tasks in a natural way. In addition, the contact forces are limited by utilizing a non-linear shape of the stiffness. Note that both of these aspects are relevant not only with respect to increased safety, but also for improving the human's contact ''feeling''. Since our approach uses an active impedance controller, it is restricted to a moderate and slow frequency domain, and thus cannot handle fast rigid impacts.

### 2.4. Combinations of Interaction and Learning

Interactive skills and imitation learning are closely related to each other (Donald 1991; Rizzolatti and Craighero 2004). However, in previous research, literature to bridge both fields is hard to find. Billard and Hayes (1998) and Billard and Dautenhahn (1998) presented a connectionist approach called DRAMA (Dynamic Recurrent Associate Memory Architecture) which allows the robot to learn communication via a teacher-following paradigm. In their method, learning to communicate is defined as that a student robot tries to achieve a similar interpretation of a situation as a teacher robot. Thus, at the end of the learning, two robots share a common vocabulary to describe their environment. However, this implies nothing but the insight into the teacher robot's sensor data. In contrast, in our proposed method, the robot learns efficiently by imitative learning during interaction with a human, because the human has a highly intelligent system to extract meaningful information from the huge spatio-temporal space. After learning motion primitives, by executing them and observing their effects (e.g. human's reactions), the robot can learn incrementally. Nakamura et al. (2005) and Takano et al. (2006) introduced a mimetic communication model for competitive HRI. Their method was implemented for the virtual fighting between a human and a humanoid robot, and was demonstrated at EXPO 2005 in Nagoya, Japan. However, pHRI in the real physical world was not addressed. After deciding which robot's motion primitive to generate, they used open-loop control, without adaptation to the changing environment in real-time.

### 2.5. Combinations of pHRI and Reasoning/ Learning

Physical interaction was included in the works of Kosuge and Hirata (2004), Billard et al. (2006), Calinon and Billard (2007), and Ijspeert et al. (2002). These works can be categorized into two groups: pHRI during motion execution and pHRI during teaching process. While interaction (i.e. force information or disturbances) was used in Kosuge and Hirata (2004) and Ijspeert et al. (2002) during the motion *execution*, Calinon and Billard (2007) and Billard et al. (2006) used physical interaction for the *teaching* (kinesthetic teaching) in a scenario of programming by demonstration.

Kosuge and Hirata (2004) developed a female dancing partner robot. In this work, force measurements were used for the recognition of a human's motion. Based on the recognition result, the robot decided the next motion using a hidden Markov process. In the work of Ijspeert et al. (2002), a dynamical system approach was used for motion primitive representation. Therein, a disturbance (e.g. by physical interaction with a human) signal was used for online modification, i.e. a stop in the time evolution, of the execution of a learned motion primitive. Calinon and Billard (2007) and Billard et al. (2006) used two ways of imitation learning: observational learning and kinesthetic teaching. By the approach of kinesthetic teaching, kinematic mapping errors from the human to the robot were corrected.

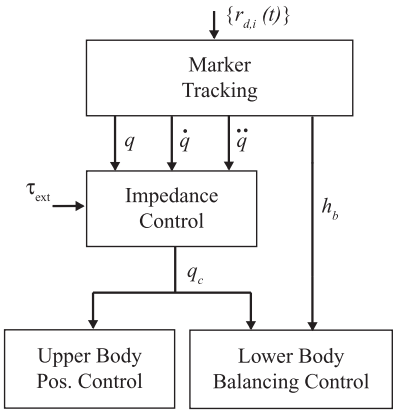


**Fig. 1.** Overview of the control strategy (Sections 3.1 and 5).

We think that in the way how physical interaction is included in our scenario differs in two fundamental ways from these previous works. First, we treat not only motion primitive learning but also learning of interaction patterns. Second, in the benchmark task considered in our work, the robot not only reacts to the physical interaction exerted by a human, but also acts to establish contact with the human. As a consequence, the physical interaction happens in two domains: the physical domain (real-time control) and the symbolic domain (learning interaction patterns), which both should be incorporated into a "complete" HRI system.

## 3. Human Motion Imitation by Marker Control

The robot's ability to imitate the human's motion is a first step for realizing the HRI tasks, which are discussed in Section 4. It allows the human to teach simple motion primitives in a preliminary step before considering physical contact in the interaction learning procedure. In this section, we present a control approach for imitating the human's motion by direct marker control. The marker trajectories can be generated by direct measurement via a motion capture system (for online motion imitation) or from the algorithm described in Section 4.6 (for motion generation). The control issues related to the physical contact will be treated later in Section 5. The overall control strategy is outlined in Figure 1. It is basically divided into marker trajectory following and impedance control for the upper body and a balancing control task for the lower body.

### 3.1. Upper Body Marker Control

The main idea of the marker tracking approach is to connect virtual translational springs between the $N$ marker positions and corresponding points on the robot (see Figure 2). When the cloud of marker points moves in space,

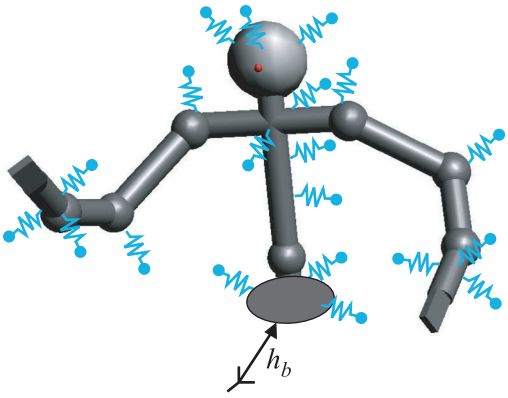


**Fig. 2.** Visualization of the marker tracking approach: virtual springs are connected between the $N = 20$ reference marker points and corresponding points on the humanoid robot.

the robot's motion will be guided by the forces generated from these springs. The direct implementation of these forces via the robot's motor torques would require a precise torque control interface, either based on motor current or torque measurement. Despite the benefits of torque measurement as demonstrated in the systems developed by DLR (Hirzinger et al. 2002; Ott et al. 2006) and ATR and Sarcos (Cheng et al. 2006), torque sensors are still not widely used. The performance of torque control via motor current measurements, on the other hand, is considerably affected by the quality of friction compensation. As a consequence, instead of implementing the virtual springs directly, we let them act on a simplified simulation of the robot upper body dynamics including a free-floating base link. In this section, it is assumed that the joint angle trajectory resulting from this simulation is commanded to a lower-level position controller (i.e. without the impedance controller in Figure 1). In Section 5.1, we use this trajectory instead as a virtual equilibrium trajectory for an underlying impedance controller as shown in Figure 1.

Let $q \in \mathbb{R}^n$ be the $n$ joint angles of the upper body. The motion of the base link is described by the base link frame $h_b \in \mathrm{SE}(3)$ and the corresponding "body twist" $\xi \in \mathrm{se}(3)$ (Murray et al. 1994)[1]. Then, we simulate a simple dynamics according to the second-order differential equations[2]

$$\dot{h}_b = h_b \tilde{\xi}, \tag{1}$$

$$M(q)\begin{pmatrix} \ddot{q} \\ \dot{\xi} \end{pmatrix} + C(q, h_b, \dot{q}, \xi)\begin{pmatrix} \dot{q} \\ \xi \end{pmatrix} = \begin{pmatrix} \tau \\ f \end{pmatrix}, \tag{2}$$

where $M(q) \in \mathbb{R}^{(n+6)\times(n+6)}$ represents a chosen (i.e. desired) symmetric and positive-definite joint-level inertia matrix including the inertia of the free-floating base link and $C(q, h_b, \dot{q}, \xi)$ is a corresponding "Coriolis and centrifugal matrix". The virtual springs then generate the joint torques $\tau \in \mathbb{R}^n$ and the six dimensional force–torque vector $f \in \mathrm{se}^*(3)$ acting on the base link. Note that, since (2) is only a simulated dynamics, it is not necessary to choose $M(q)$ as the real robot's inertia, but it can be a simple diagonal matrix as well.

The virtual springs between the $N$ marker positions $r_{d,i}$ and corresponding points on the simulated humanoid $r_i(q, h_b)$ are generated via the potential functions $V_i(q, h_b) = \frac{1}{2} k_i \parallel r_{d,i} - r_i(q, h_b) \parallel_2^2$ where $k_i \in \mathbb{R}$ represents the stiffness of the virtual spring. The generalized forces $\tau$ and $f$ according to these springs can be computed via the differential of the potential functions. By summarizing the marker forces over the set $\mathcal{M}$ of visible markers, and adding an additional damping term with damping matrix $D(q)$, we obtain

$$\begin{pmatrix} \tau \\ f \end{pmatrix} = -D(q)\begin{pmatrix} \dot{q} \\ \xi \end{pmatrix} + \sum_{\forall i \in \mathcal{M}} k_i J_i^{\mathrm{T}}(q)\big(r_{d,i}(t) - r_i(q, h_b)\big), \tag{3}$$

where $J_i(q)$ is the Jacobian matrix according to the position $r_i(q, h_b)$. The position-dependent damping matrix $D(q)$ should be chosen such that the dynamics (2) in combination with the stiffness term in (3) is well-damped. Therefore, we adopt a method called "double-diagonalization", which was used in Albu-Schäffer et al. (2003) in the context of impedance control and is based on the generalized eigenvalue problem for symmetric matrices (Harville 1997). Since the inertia matrix $M(q)$ is a symmetric and positive-definite matrix and the effective stiffness matrix $K := \sum_{\forall i \in \mathcal{M}} k_i J_i^T(q) J_i(q)$ is symmetric and positive semi-definite, the generalized eigenvalue problem allows us to find (numerically) a non-singular matrix $Q(q)$, such that $M(q) = Q^{\mathrm{T}}(q)Q(q)$ and $K(q) = Q^{\mathrm{T}}(q)K_0(q)Q(q)$ with a diagonal matrix $K_0$. Then, the damping matrix is chosen as $D(q) = 2\zeta_d Q(q)^{\mathrm{T}} diag(\sqrt{(K_{0,i})})Q(q)$ with a damping factor of $\zeta_d = 0.7$ for a well-damped behavior (Ott et al. 2008).

Note that the common problem of missing marker data is handled in this setting by simply omitting the non-visible markers from the summation in (3). However, in the case of the online imitation from the motion capture system, the problems related to incorrect marker labeling and the possibility that markers are detaching from the human cannot be directly handled by the presented controller and must be treated by an additional software safety layer.

In order to avoid hardware limits, a modification of (3) is required. A repellent joint torque $\tau_{l,i}$ is added to $\tau_i$ when the angle comes close to a hardware limit. For the implementation, we chose the contact model proposed by Hunt and Crossley (1975) with a (dimensionless) shape parameter of 1 and a stiffness which was set considerably higher than the diagonal element of $K$ for each joint (Ott et al. 2008). The repellant force becomes active if the joint is closer to the joint limit than a safety distance $\delta$ and is given by

$$\tau_{l,i} := \begin{cases} -k_{l,i}(q_i - q_{M,i}) - d_{l,i}|q_i| - q_{M,i}|\dot{q}_i & q_i > q_{M,i} \\ k_{l,i}(q_i - q_{m,i}) - d_{l,i}|q_i - q_{m,i}|\dot{q}_i & q_i < q_{m,i} \\ 0 & \text{otherwise} \end{cases}$$

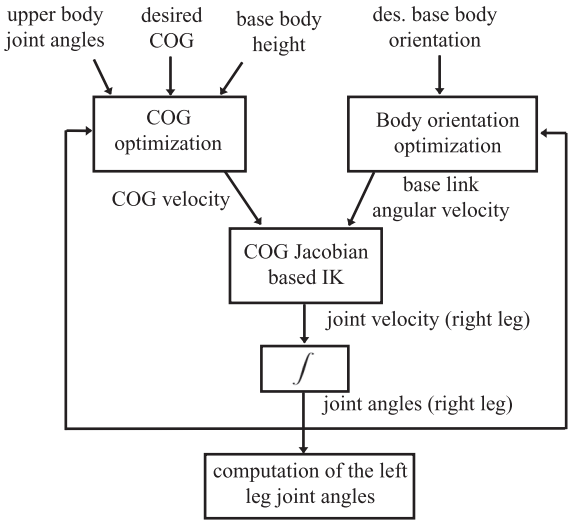


**Fig. 3.** Lower body balancing algorithm.

where $q_{M,i} = q_{i,\max} - \delta$ and $q_{m,i} = q_{i,\min} + \delta$. According to Hunt and Crossley (1975) and Marhefka and Orin (1999), the damping gains are set to $d_{l,i} = 3/2\zeta k_{l,i}$ and the damping factor is chosen as $\zeta = 0.7$. Note that the damping of the hardware limit implementation is not chosen according to the above-mentioned "double-diagonalization" damping design but according to the contact model of Hunt and Crossley, because this ensures that both the stiffness and the damping force remain continuous when the joint angle crosses the points $q_{i,\max} - \delta$ or $q_{i,\min} + \delta$.

### 3.2. Lower Body Balancing Control

The algorithm of the previous section is applied only to the motion of the robot's upper body (waist, arms, and neck). Instead, the role of the leg joints is twofold. On the one hand, the legs are supposed to ensure the balancing of the whole robot, while the arms are following the marker trajectories. In addition to this, the motion of the base link $h_b$ must also be realized via the joints of the legs, since the hip position and orientation depend on the joint configuration of the legs. By handling the balancing task separately in the control of the lower body, we achieve an accurate imitation of the human's arm and upper body motion without any influence on the balancing constraints. The balancing algorithm is outlined in Figure 3. It is based on a velocity-level inverse kinematics for the center of gravity (COG) and the base link orientation. In particular, the COG displacement from the desired point due to the upper body motion should be compensated for. Therefore, a simple optimization is used for computing a compensating "COG velocity" taking account of the current upper body configuration and the desired height of the base link. In this algorithm, we assume that during the motion both feet keep in contact with the ground, i.e. we currently do not treat stepping motions. Therefore, we only have to solve for the joint angles of one leg directly, while the configuration of the other leg can be obtained in a second step from the closed kinematic loop. For a more detailed description of the balancing algorithm, the interested reader is referred to Ott et al. (2008). Note that Nakaoka et al. (2005) proposed a more complicated balancing algorithm which also includes stepping motions, but their algorithm does not allow online execution.

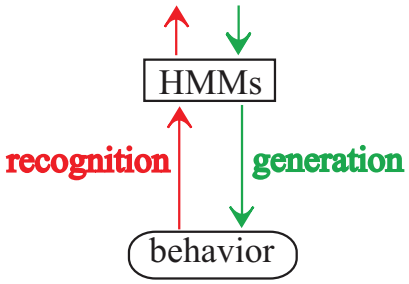


**Fig. 4.** Mimesis model. Hidden Markov models are used for bidirectional computation of recognition and generation of motion patterns.

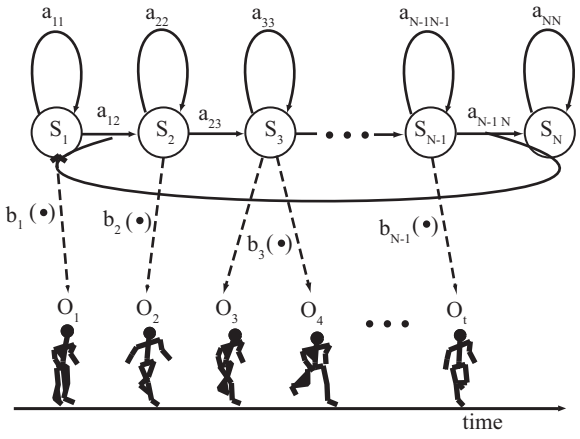


**Fig. 5.** Periodic continuous Hidden Markov model. Here, $s_i$ represents the $i$th state and $a_{ij}$ represents the probability of transition from the $i$th state to the $j$th state. The term $b_i(x)$ represents the probability of generating $x$ from the $i$th state.

## 4. Mimetic Communication

### 4.1. Mimesis Model

With the baseline of the motion imitation (Section 3), a framework for motion learning, recognition, and generation was proposed by Inamura et al. (2004), which is called the "mimesis model". In this section, we give a brief overview of this concept, because it will be fundamental for the remaining part of the paper. From motion data, motion primitives are learned in a compact representation. By using the learned motion primitives, motions of another agent (a human or a humanoid) are recognized. From the learned motion primitives, self-motions can be reproduced at anytime without the help of another agent. We use the mimesis model shown in Figure 4 which

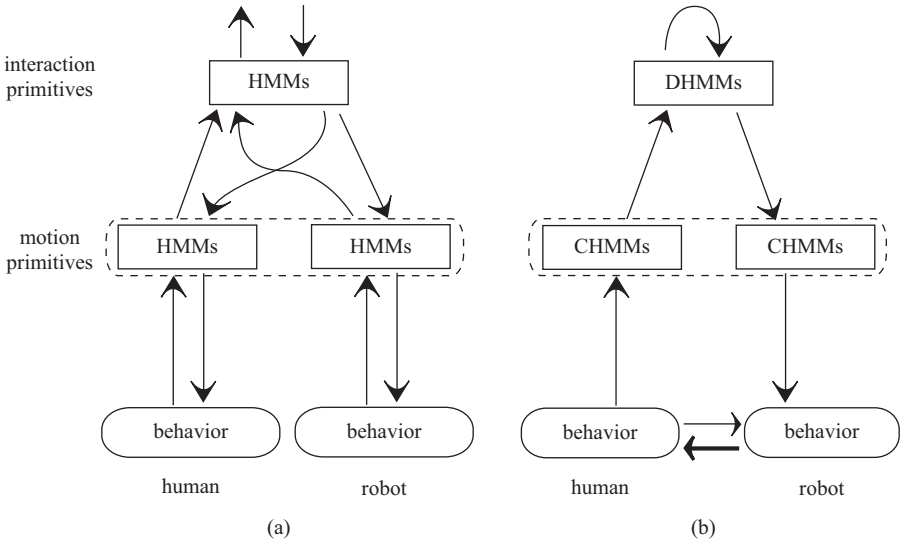


**Fig. 6.** Mimetic communication model: (a) the prototype model and (b) the modified model in this research

fulfills these properties. It is a bidirectional computational model, which is inspired by the mirror neuron system (Rizzolatti et al. 1996), with the concept of motion primitives.

The advantages of using motion primitives are summarized as follows.

- The use of motion primitives leads to a compact representation of motions and thus is an efficient computational strategy.
- Learned motion primitives are easy to reuse for recognition of other's motions and the generation of self-motions.

For motion primitive representation, the HMM shown in Figure 5 is adopted because it provides a concise stochastic representation of spatiotemporal patterns and has well-established computational methods (Rabiner 1989). A HMM $\lambda$ is represented by the following variables:

- $S$, the finite set of the states of the HMM, $S = \{s_i\}$, $1 \leq i \leq N$, where $N$ is the number of states of the model; $q_t$ denotes for the state at time $t$;
- $\pi$, the initial state probabilities vector $\pi = \{\pi_i\}$, $1 \leq i \leq N$; the parameter $\pi_i$ is $P[q_1 = s_i]$, the probability for the initial state $q_1$ to be $s_i$;
- $A$, the state transition probability matrix $A = \{a_{ij}\}$, $1 \leq i,j \leq N$, where $a_{ij}$ is $P[q_{t+1} = s_j | q_t = s_i]$, the probability of transition from state $i$ to state $j$;
- $B$, the observation symbol probability distribution. $B = \{b_i\}$, $1 \leq i \leq N$; $b_i(o)$ is the probability density function for the output of a vector $o$ at the $i$th state node.

While the original mimesis model of (Inamura et al. 2004) was designed in joint space, in this paper we perform learning, recognition, and generation of motion primitives in Cartesian marker coordinates paving the way for extending these concepts to task-space problems and object manipulation (Lee et al. 2008b).

### 4.2. Mimetic Communication Model

Figure 6(a) explains the principle of the mimetic communication model for interaction (Nakamura et al. 2005), which is a hierarchical model consisting of three mimesis models. The two groups of HMMs in the lower layer represent "motion primitives" for a robot and a human and they are shared by both the robot and the human. The upper layer HMMs represent "interaction primitives"[3]. In Figure 6(a), the two recognition outputs of the mimesis models in the lower layer become the recognition input of the mimesis model in the upper layer. The recognition output in the upper layer is the estimated interaction primitive. From an interaction primitive, a sequence of interactive motion primitives of two subjects is generated. In Nakamura et al. (2005) and Takano et al. (2006), a simplified model was implemented for their experiments which was designed for interaction in a virtual world.

Similar to Nakamura et al. (2005) and Takano et al. (2006), in this paper the hierarchical design of mimetic communication model is adopted because the interaction patterns can be represented as a sequence of motion primitives, which provides a more compact representation and better modularity. Precisely speaking, the modified model shown in Figure 6(b) is used. The motion primitives in the lower layer are represented as continuous HMMs (CHMMs) and the interaction primitives in the upper layer HMMs are represented as discrete HMMs (DHMMs)[4]. The human behavior is recognized by using motion primitives. From the recognition output of the human's behavior, the interaction pattern is recognized by using interaction primitives[5]. The recognized interaction primitive is taken as the

high-level controller for interaction, which decides an appropriate motion primitive for the robot to perform. Then, from the selected motion primitive, a reference trajectory of the robot behavior is generated. Further, the robot reference trajectory is modified to adapt to the real human motion in the physical world with a lower sampling time (the thin horizontal arrow, the details are given in Section 5). Also, the human adapts their behavior to the real humanoid behavior in real time (the bold horizontal arrow), which is not computationally implemented but naturally embodied. Although in principle an expected motion primitive of the human can also be calculated, this is not used because the robot cannot control the human behavior directly. In the future, however, it might be interesting to use the expected human behavior for influencing the human behavior indirectly.

There are several differences between the mimetic communication model in Nakamura et al. (2005) and Takano et al. (2006) and the proposed method. First, in contrast to these works, pHRI in the real physical world is realized. Second, while the approach in Takano et al. (2006) used an open-loop control after selecting which robot's motion primitive to generate, in our method physical contact information is learned and used for adaptation of motion primitives in real-time. Third, the interaction primitives are embodied into different formats: CHMMs in Takano et al. (2006) and DHMMs in our method. Fourth, the interactive motions between a subject and their partner are represented in a different style. In the proposed method, contact information and the labels of actions and reactions are used for representation of an interaction primitive. The trajectories of two subjects in proto-symbol spaces[6] which are constructed based on the Kullback–Leibler information (Rabiner 1989) by using the multidimensional scaling method (Cox and Cox 2001) are used in Takano et al. (2006). Fifth, different learning approaches are used. While the interaction was done by observing interactive humans in (Takano et al. 2006), in the proposed method the robot learns interaction primitives in a way in which it is actively involved in the learning process. The details are explained in Section 4.4.

## 4.3. Motion Primitive Training

The demonstrator motion is usually observed by using a motion capture system. Motion learning means motion primitive acquisition that involves segmentation of observed motion data and stochastic modeling of each segment. Segmentation algorithms may be found in (Janus and Nakamura 2005; Fod et al. 2002; Takano and Nakamura 2006; Kulić et al. 2008). The inherent dynamics of a segmented motion is represented as a HMM, the parameters of which are optimized by the expectation maximization (EM) algorithm (Dempster et al. 1977). At the current stage, in our experiments, the training data set is segmented manually during the learning process. However, our method can be extended to be fully autonomous in the learning stage by integrating an autonomous online segmentation algorithm (Kulić et al. 2008). Since both the algorithm of Kulić et al. (2008) and our proposed work are built on top of the mimesis model (Inamura et al. 2004), they can be integrated easily.

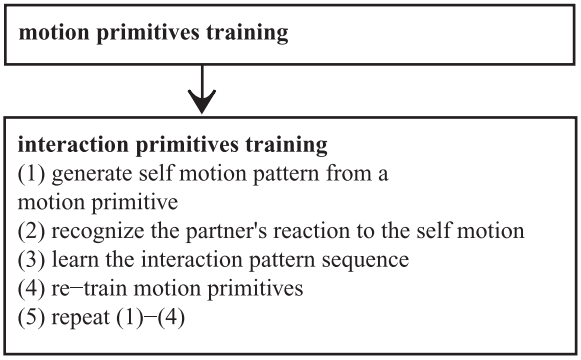


**Fig. 7.** Interaction primitive learning procedure.

Since the kinematics models and joint limits are different between the robot and the human, the trajectories of human motion patterns are not guaranteed to be performable for the robot. In order to ensure that motion patterns, which the robot can perform kinematically, are used in the training, an approach of learning by imitation is adopted, rather than learning from observation. More precisely, we make the robot follow the human motion patterns using the direct marker control method described in Section 3. Only well-tracked motion patterns are used as training data sets for motion primitives training. Currently, whether a motion pattern is well-tracked or not is judged manually by the demonstrator. Since a human demonstrator is involved in the teaching, we interpret this as teacher's feedback and we do not consider this as a major limitation. However, the selection of well-tracked patterns can be done automatically by checking the tracking errors and joint hardware limits easily.

Based on global marker measurements on the human base link, the human base link frame is calculated in a closed form using Horn's method (Horn 1987)[7]. Then, all markers' positions are transformed into the current base link frame and the human base link frame is transformed into the initial base link frame. The time series of transformed Cartesian positions of markers and the base link position/orientation are encoded in periodic continuous HMMs as shown in Figure 5.

## 4.4. Interaction Primitive Training

Interaction can be learned in two ways: learning by observation and learning by active involvement. The first approach, which is adopted in Takano et al. (2006), is learning interaction patterns from observing the interaction of two humans from the outside. The other approach, which is adopted in this paper, takes an active learning strategy where the robot is involved in demonstration of interaction

**Fig. 8.** Two types of hand correspondence: (a) the same hands (right–right, left–left) of self and partner are corresponding; (b) opposite hands (right–left, left–right) of self and partner are corresponding.

patterns. To be specific, the robot performs a learned motion pattern, observes the partner's reaction to the generated motion pattern, and recognizes the partner's motion. Thereby, the causality of motions (i.e. the pair of self-action and the other's reaction) is learned. In this way, previously learned knowledge is reused for acquiring new knowledge (the causality of the motions, such as interaction primitives), and the learning mechanism becomes interactive and incremental.

Moreover, another advantage of this active involvement strategy is that additional important sensory information can be collected. When watching two people's "high five" motions, the robot cannot perceive the cutaneous sensory information (e.g. contact forces). In contrast, if the robot is actively involved in the learning procedure, this data can also be acquired in addition to the visual sensory data. Currently, the embodiment of cutaneous sensation into the symbolic domain has not yet been implemented. However, since coupling of the two media (cutaneous sensation and sight sensation) causes interesting effects for communication, we will take a closer look at this issue in our future work.

Figure 7 explains an overview of the interaction primitive training procedure, which follows the learning of motion primitives (Section 4.3).

**Step 1** The robot replays a motion pattern, generated from a learned motion primitive[8].

**Step 2** The human partner reacts to the robot behavior. We assume that the partner's behavior is cooperative. By using the learned motion primitives, the partner's reacted behavior is recognized by calculating the likelihood for each learned motion primitive (HMM) and finding the HMM which has the highest likelihood.

**Step 3** The sequence of the self- (robot) motion primitive label, the partner (human) motion primitive label, and the information where contact occurs is encoded into a left-to-right type discrete HMM via the EM algorithm (Rabiner 1989). The information where contact occurs is represented as the contact hand correspondence between the human and the robot. The details are explained in the following paragraph.

**Step 4** After learning the interaction primitive, further interaction information (e.g. when contact occurs) is learned. The contact timing is represented indirectly as the distance trajectories of the robot's hands and the partner's corresponding hands, because the distance information gives an idea when to make contacts. The distance trajectories are added into the previously learned motion primitives. Previously optimized HMM parameters are not modified. Since we are adding new elements (distance information between corresponding hands) into the HMM, corresponding parameters (to be precise, the output emission probability for the new output elements) should be added and optimized. Such optimization is done by the following modification of Viterbi training. The optimal state transition is found for the training data and, then, only the output emission probability for the new output elements is updated. In order to achieve accurate physical interaction, the distance information is used for adaptation of the robot's trajectory. The implementation details are given in Section 5.2.

**Step 5** The processes of Steps 1–4 are repeated for all of the trained motion primitives.

At the current stage, physical interaction is limited to hand contacts and the type of hand correspondence is limited to two types as shown in Figure 8. In the first type (Figure 8(a)), the right (left) hand of subject 1 and subject 2 correspond to each other. In the second type (Figure 8(b)), the right (left) hand corresponds to the left (right) hand of the partner. Positional correspondences $corr_{ij}(t)$ of the self hands $p_{1i}(t)$ to the partner hands $p_{2j}(t)$ are calculated by

$$corr_{ij}(t) = p_{1i}(t)^{\mathrm{T}} p_{2j}(t) - p_{1i}(1)^{\mathrm{T}} p_{2j}(1) \qquad (4)$$

where $i$ and $j$ denote a label for the right or left hand, respectively. By comparing the values of the heuristic distance measures

$$\chi_1 := \int_{t=0}^{T} (corr_{RR}(t) + corr_{LL}(t))\, dt$$

and

$$\chi_2 := \int_{t=0}^{T} (corr_{RL}(t) + corr_{LR}(t))\, dt,$$

where $T$ denotes the duration of the motion primitive, the effector correspondence type can be distinguished. For $\chi_1 > \chi_2$, the contact pairs between the robot and the partner are identified as the same hands (right–right and/or left–left) as depicted in Figure 8(a). In Figure 9, trajectories

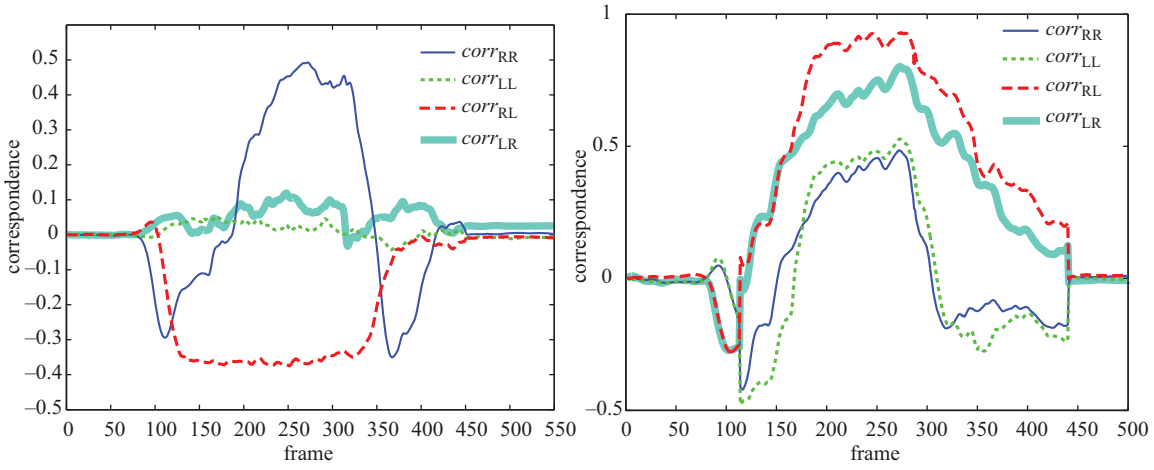


**Fig. 9.** Poitional correspondence between robot hands and human hands. Left: During a right-hand high five motion, same hands (right–right, left–left) of self and partner are corresponding. Right: During a high ten motion, opposite hands (right–left, left–right) of self and partner are corresponding.

of $corr_{RR}$, $corr_{LL}$, $corr_{RL}$, and $corr_{LR}$ are depicted during a high five and a high ten interaction between a human and a robot. In the case of the high five interaction (left part of Figure 9), the value of $\chi_1$ was 34.7550 and the value of $\chi_2$ was $-66.1084$, which implies that the correspondence of the same hands (right–right, left–left) of self and partner is higher than that of opposite hands. On the other hand, in the case of the high ten interaction (right part of Figure 9), the value of $\chi_1$ was 30.7665 and the value of $\chi_2$ was 323.2609.

Since hands are used the most frequently for interaction with objects and other humans, we start with physical interaction with hand contacts first. However, this does not limit the generalizability of our presented approach. By simply increasing the number of possible contact candidates, this method can be extended for physical interactions using more body parts. In order to generalize the approach to most motions, the recognition of contact type should be generalized, instead of using a heuristic function such as (4). A possible way to upgrade the proposed method to a general solution is to apply a method of constraint learning (Calinon and Billard 2008; Kunori et al. 2009).

## 4.5. Recognition

We distinguish between recognition of motion patterns and recognition of interaction patterns. The basic mathematical formulas are the same as for the identification of the HMM $\lambda^*$ that has the highest likelihood to the input pattern $O = [o_1, o_2, \ldots, o_T]$.

$$\lambda^* = \arg\max_{\lambda} P(O|\lambda). \tag{5}$$

The likelihood $P(O|\lambda)$ indicates the probability that a motion pattern $O$ is generated by an HMM $\lambda$. We compute $P(O|\lambda)$ for each HMM among the pre-trained HMMs by the forward algorithm (Rabiner 1989). The HMM that provides the highest $P(O|\lambda)$ is the result of motion recognition.

For the motion primitive recognition, the input pattern consists of the markers' Cartesian positions and the base link position/orientation. Please note that the measured distances between human hands and corresponding robot hands are not used for recognition because hand correspondence is unknown before recognizing the interaction primitive.

For the interaction primitive recognition, the input pattern is a time series of recognized motion primitives of the human behavior, as shown in Figure 6(b). Since the interaction primitives contain information about action, reaction, and hand correspondence, one can see that the input data for the interaction recognition is incomplete (or "partial") data[9]. The missing elements (invisible markers, the sequence of robot motion primitives, and hand correspondence type) are handled by adopting the algorithm of "motion recognition from partial observations" (Lee and Nakamura 2005), applied to both motion recognition and interaction recognition.

## 4.6. Generation

The recognized interaction primitive is considered as the high-level interaction strategy for the robot. From the recognized interaction primitive, the interaction pattern is decoded. The interaction pattern consists of the human motion primitive label, the robot motion primitive label $l$, and the hand correspondence type $c$.

From the robot motion primitive label $l$, a motion pattern for the humanoid robot is decoded. The decoded motion pattern consists of marker positions to track, base link position/orientation, and reference distances between robot hands and corresponding human's hands. According to the effector corresponding type $c$, the corresponding human hand positions to the robot hands are known. The real positions of corresponding human hands during interaction are captured and transformed into the robot base link frame (Horn 1987).

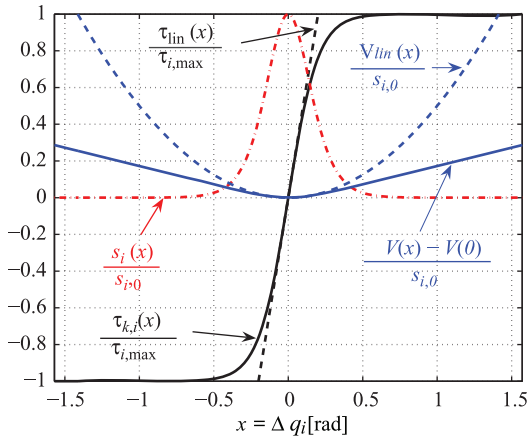


**Fig. 10.** Shape of the "non-linear stiffness term" $\tau_{k,i}(\Delta q_i)$ (black solid line) used in (6), compared with a linear stiffness term $\tau_{\text{lin}} = s_{i,0}\Delta q_i$ (black dashed line) for the case $k_{i,0} = 100\text{Nmrad}^{-1}$ and $\tau_{i,\max} = 20\text{Nm}$. The stiffness at equilibrium is given by $k_{i,0}$ and the output torque is limited by $\tau_{i,\max}$. The figure also shows the shape of the potential function for the chosen stiffness term $V(\Delta q_i)$ (solid) in comparison with the potential of the linear stiffness term $V_{\text{lin}}(\Delta q_i) = \frac{1}{2}s_{i,0}\Delta q_i^2$ (dashed). In addition, the dashed-dotted line shows the shape of the effective stiffness $s_i(x) := \partial\tau_{k,i}(x)/\partial x$.

Thereafter, the trajectories of the marker position $r_{d,i}$, the base link frame $h_b$, the reference distances $d_{r,k}$ between corresponding hands, and the real positions of corresponding human hands for contact are commanded to the robot. While the trajectory of the marker position $r_{d,i}$ becomes the input of the upper body marker control (Section 3.1) and the base link frame motion $h_b$ becomes the input of the lower body balancing control (Section 3.2), the other components are used for real-time adaptation in Section 5.2.

## 5. Physical Human–Robot Interaction

Our strategy for handling the physical contact between the human and the robot has two aspects.

1. The robot's behavior is made compliant during all of the motions by applying (position-based) impedance control.
2. The motion from the marker control algorithm is adapted to the actual human's hand position in real-time based on learned contact information (e.g. when and where contacts occur).

### 5.1. Impedance Control

In Section 3.1, it was assumed that the trajectory $q$ resulting from (2) is implemented with a position controller for the joints of the upper body. With regard to the pHRI, we use $q$ now as the virtual equilibrium trajectory for a position-based impedance controller (respectively, admittance controller), see Figure 1. In the design of the impedance controller, particular emphasis is put on limiting the contact forces for allowing safe and "smooth" HRI. The impedance behavior will be designed as a joint-level impedance with $q_c$ denoting the output joint angles commanded to the robot's joint position controllers. Consequently, we transform the measured generalized Cartesian forces $F_{EF,r}$ and $F_{EF,l}$ at the end-effectors into external joint torques $\tau_{\text{ext}}$ via the transposed of the relevant Jacobian matrices $J_r(q_c)$ and $J_l(q_c)$, respectively. Since $\tau_{\text{ext}}$ serves as an estimate for the external joint torques, one should remove the dynamical forces due to the robot's own motion from the sensor measurements. However, up to this time, in the experiments reported in Section 6, we only remove the static gravity forces, while we neglect the inertial forces.

With the notation $\Delta q = q - q_c$ for the deviation of $q_c$ from the virtual equilibrium $q$, the used joint-level impedance behavior can be formulated as

$$M_I\Delta\ddot{q} + D_I(\Delta q)\Delta\dot{q} + \tau_k(\Delta q) = \tau_{\text{ext}}, \tag{6}$$

where $M_I \in \mathbb{R}^{n\times n}$ is a constant diagonal matrix containing the desired joint inertia values and $D_I(\Delta q) \in \mathbb{R}^{n\times n}$ is a joint level damping matrix. Furthermore, the stiffness term $\tau_k(\Delta q) = \{\tau_{k,i}(\Delta q_i)\} \in \mathbb{R}^n$ is chosen by the functions

$$\tau_{k,i}(\Delta q_i) := \tau_{i,\max}\tanh\left(\frac{s_{i,0}}{\tau_{i,\max}}\Delta q_i\right) \quad \forall\ i = 1,\ldots,n, \tag{7}$$

which are based on the tangens hyperbolicus function[10] such that the stiffness value $s_i(\Delta q_i) = \partial\tau_{k,i}(\Delta q_i)/\partial\Delta q_i$ at the free equilibrium is given by the parameter $s_{i,0}$ and the torque $\tau_{k,i}(\Delta q_i)$ is limited by the parameter $\tau_{i,\max}$ (see Figure 10). This limitation of the stiffness force has the consequence that the corresponding potential function grows linearly for large deviations and the local stiffness $s_i(\Delta q_i)$ goes to zero as $\Delta q_i$ goes to infinity.

For the design of the damping matrix, the non-linear shape of the stiffness term should be taken into account, while the inertia matrix $M_I = \text{diag}(m_i)$ in (6) is a constant diagonal matrix. Since the damping matrix $D_I(\Delta q)$ can be any positive-definite matrix, we use a linear design, which is derived from the linearization of (6) at $\Delta q_i$. In this linearization, the stiffness is given by $s_i(\Delta q_i)$ (Arnold, 1989) and consequently the damping matrix is taken as

$$D_I(\Delta q) = \text{diag}\left(2\xi_I\sqrt{m_i s_i(\Delta q_i)}\right), \tag{8}$$

with the damping factor set to $\xi_I = 0.7$ for a well-damped behavior. Note that by this choice the damping goes to zero for large deviations, since it is computed based on the local differential $\partial\tau_{k,i}(\Delta q_i)/\partial\Delta q_i$ (see Figure 10). If this is not desired, an alternative choice would be to use the difference $\tau_{k,i}(\Delta q_i)/\Delta q_i$ instead of $s_i(\Delta q_i)$ in (8). However, for the experiments reported in Section 6, we used (8).

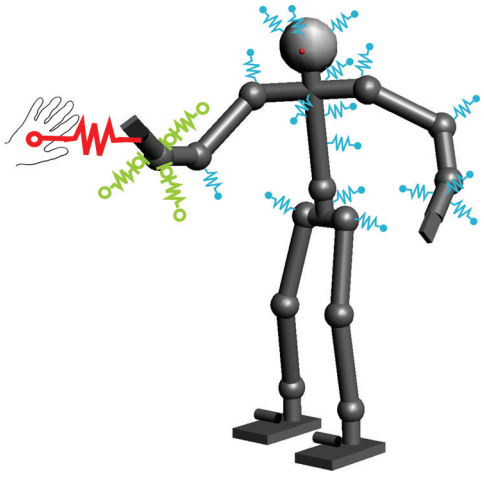

**Fig. 11.** Sketch of the interactive marker trajectory following: In order to achieve an exact contact with the human's hand position, an additional spring is attached to the robot's end-effector (large bold spring) and the forces from the marker springs connected to the hand (thin large springs) are projected into a subspace related to the end-effector torques.

## 5.2. Realization of the Expected Human–Robot Contacts

The mimetic communication model in Section 4 allows us to recognize a human motion pattern, to select an appropriate interaction strategy, and to generate an appropriate robot motion pattern ($r_{d,i}$ and $h_b$). The control algorithm presented in Section 3 allows us to follow a commanded marker trajectory ($r_{d,i}$ and $h_b$) in real-time and, by utilizing the impedance controller from Section 5.1, to react to external forces in a compliant way. However, simply following the marker trajectory $r_{d,i}$ and base link motion $h_b$ is not sufficient in realistic scenarios. The human user will not always perform the motions in exactly the same way and will have a different pose with respect to the robot than during the learning. As a consequence, it is necessary to adapt the motion $q$ to the human's actual hand positions at the time of contact.

From a control point of view, we tackle this problem by modifying the marker control approach from Section 3.1. The idea, as sketched in Figure 11, is to attach another virtual spring between the robot's hands and the corresponding human's hands (e.g. where contacts occur) just before and during the contact (e.g. when contacts occur). The contact time information is related to the expected distance $d_{r,k}$ generated from the motion primitive. The correspondence information is provided by the mimetic communication model (Section 4.6). Note that for this, the human's hand position with respect to the robot's base link must be measured online. The robot base link frame is calculated in a closed-form by Horn's method (Horn 1987) based on marker measurements on the robot's torso. However, by simply attaching this additional spring, it is clear that this spring would have to counteract against all other marker springs attached to the robot's hand. The desired behavior instead

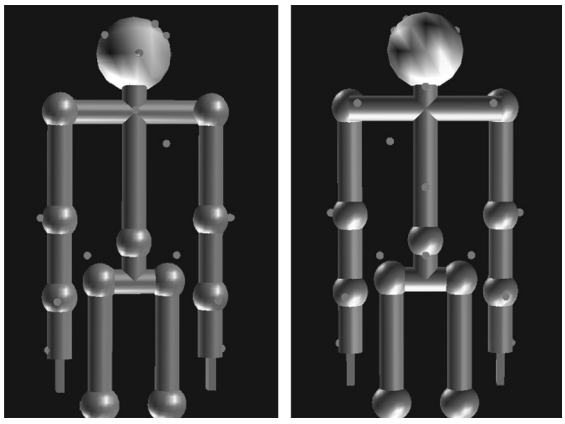

**Fig. 12.** Marker set for measuring the human's upper body motion.

is such that the robot's hand position is mainly affected by the newly added spring, while the remaining marker springs connected to the arm would rather shape the pose and the hand orientation. Therefore, we first compute the resulting force and torque of all forces from the marker springs connected to the hand (i.e. the thin large springs in Figure 11) with respect to the hinge point of the newly added hand spring. Then, during contact we project this force/torque pair into the subspace corresponding to the end-effector torques such that any effective force at this point is eliminated. Since we do not want to switch abruptly from the normal marker control to the newly added hand spring, we add weighting parameters for the forces generated by the virtual springs. The weight parameter for the newly attached spring (the large bold spring in Figure 11) is $\delta_k$ and the weight parameter for the thin large springs in Figure 11 is $1 - \delta_k$. Note that $k$ denotes a label for the robot's right ($k \rightarrow r$) or left ($k \rightarrow l$) hand. The parameter is modified continuously based on $d_{r,k}$, the expected distance between the robot and human hand, because the expected contact timing can be inferred from the expected distance. For a small distance $d_{r,k}$ and during contact, $\delta_k$ is set to 1 such that the end-effector position is controlled mainly via the newly added hand spring. For a large desired distance $d_{r,k} > d_{\text{free}}$, the hand spring is deactivated by setting $\delta_k$ to zero. In between these values we interpolate linearly:

$$\delta_k := \begin{cases} 1 & d_{r,k} < d_{\min}\ [m] \\ 1 - (d_{r,k} - d_{\min})/(d_{\text{free}} - d_{\min}) & d_{\min} \leq d_{r,k} \leq d_{\text{free}} \\ 0 & d_{r,k} > d_{\text{free}}\ [m] \end{cases}$$

In the experiments reported in Section 6, we set $d_{\min}$ to 20 cm and $d_{\text{free}}$ to 35 cm such that the generated motion primitive is modified only in the period where the desired distance is smaller than 35 cm.

Let $F_{w,k} \in \mathbb{R}^3$ and $T_{w,k} \in \mathbb{R}^3$ denote the resulting Cartesian force and torque from the marker springs connected to the right ($k \rightarrow r$) and left ($k \rightarrow l$) hand (respectively,

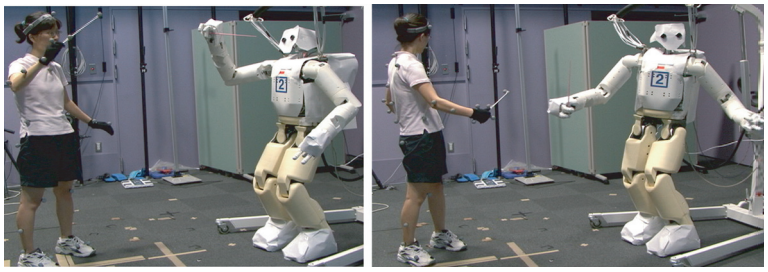

**Fig. 13.** Real-time motion imitation by direct marker control of a 4-beat conductor and waist twisting motion (see also Extension 1).

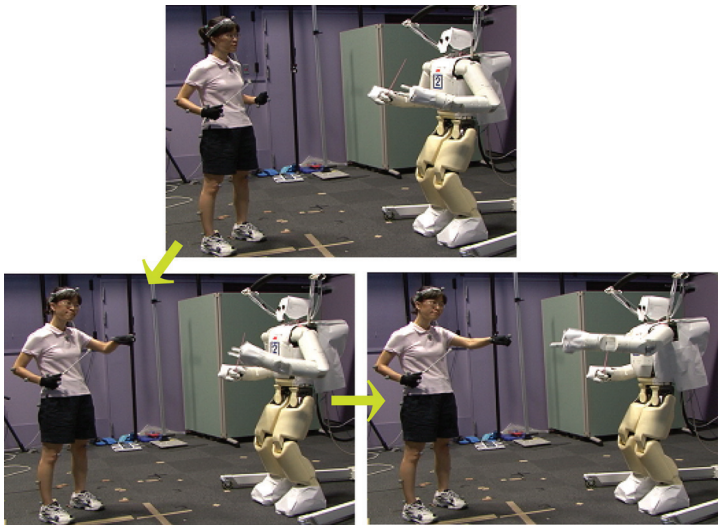

**Fig. 14.** Sequence of a *Punch* motion, by online direct marker control (see Extension 1).

wrist). Furthermore, let $F_{h,k} \in \mathbb{R}^3$ be the force according to the springs between the human's hands and the robot's right ($k \to r$) and left ($k \to l$) hand. Then, the procedure as described above can be implemented by using the control law

$$\begin{pmatrix} \tau \\ f \end{pmatrix} = -D(q)\begin{pmatrix} \dot{q} \\ \xi \end{pmatrix} + \sum_{\forall i \in \mathcal{M}\setminus\mathcal{H}} k_i J_i^{\mathrm{T}}(q)\left(r_{d,i}(t) - r_i(q, h_b)\right) + \sum_{k=r,l} J_{h,k}^{\mathrm{T}}(q)\begin{pmatrix} \delta_k F_{h,k} + (1-\delta_k)F_{w,k} \\ T_{w,k} \end{pmatrix},$$

instead of (3), where $\mathcal{H}$ denotes the set of markers connected to the hands and $J_{h,k}(q)$ the Jacobian matrices of the right ($k \to r$) and left ($k \to l$) hand frames. The parameters $\delta_r \in \mathbb{R}$ and $\delta_l \in \mathbb{R}$ have values between 0 and 1 and vary with the desired distance between the robot's and the human's hands.

In this section, we explained how to adapt the motion primitives which are generated from HMMs for the physical contact establishment. We would like to emphasize that this motion primitive adaptation is the result of coupling between control and learning mechanism. The marker controller is modified based on learned contact information (e.g. where and when contacts occur).

## 6. Experiments

The proposed algorithms have been implemented on the IRT humanoid robot shown in Figure 13. This robot has 38 degrees of freedom, consisting of 3 joints actuating the head, 7 joints in each of the arms, 6 joints in each of the legs, 1 joint at the waist, 3 joints in each of the hands actuating the fingers, and 1 joint for each toe. During the experiments, the degrees of freedom in the fingers and toes were not used. Namely, 30 degrees of freedom were controlled.

The robot is controlled from two real-time computers connected via a network: one for the upper and the other for the lower body. The marker trajectory is sent in real-time to the upper-body computer via a UDP socket interface. The control algorithms from Sections 3 and 5 are implemented on these computers with a sampling rate of 2 ms. The damping design is computationally expensive and was performed at a lower rate of 50 ms.

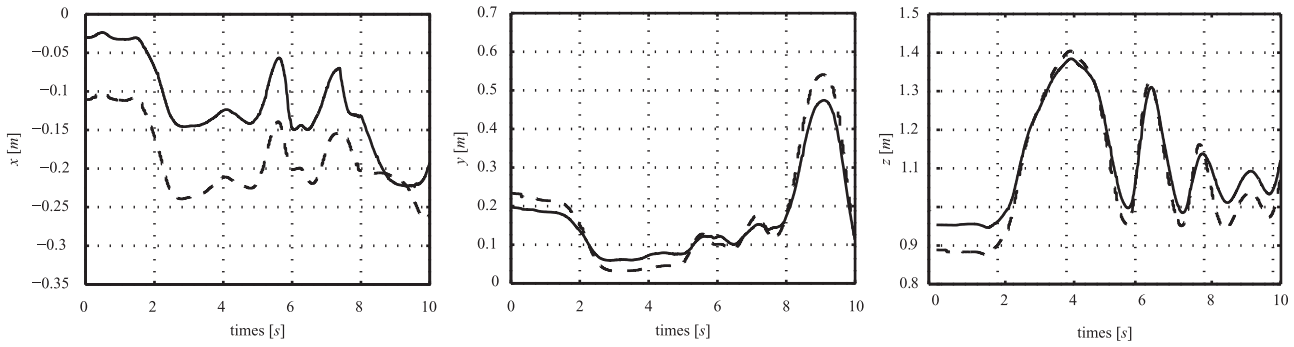


**Fig. 15.** Position of marker 1 on the right wrist. The dashed line shows the measured marker position on the human, and the solid line shows the motion of the corresponding point of the robot.

## 6.1. Evaluation of Online Direct Marker Control

A set of 34 markers were attached on the human and 2 additional markers were attached on a conductor stick. Only the 20 markers on the human upper body, shown in Figure 12, were used for the control and motion recognition algorithm. The motion capture system captures the Cartesian positions of the markers with a sampling rate of 10 ms. In this experiment all stiffness values of the marker springs were chosen as 1,000 N $m^{-1}$ and the inertia matrix $M(q)$ was chosen diagonal and constant.

We tested the direct marker control algorithm from Section 3 with conductor-like motions and punch motions of the arms as well as bowing and squat motions. Figures 13 and 14 show some snapshots of the action. A video of these motions can be seen in Extension 1. The trajectories of two markers attached to the right hand during one of the 4-beat conductor motions are shown in Figures 15 and 16. The dashed lines show the measured data from the motion capture system which is used as a desired trajectory for the controller. The solid lines show the resulting motion of the corresponding points on the robot. The correspondence is only approximative by nature, due to considerable kinematic differences between the human and the robot as well as due to imprecise marker placement. Therefore, one cannot expect the errors to go to zero exactly even in steady state. Instead, the controller basically minimizes the overall distance to all of the marker points according to the chosen stiffness values $k_i$ from (3). On the other hand, one can see that the overall motion is well preserved.

## 6.2. Evaluation of Mimesis Model in Task Space

A large data set (about 27 minutes) of a variety of whole body motions was collected in the motion capture studio. From the global Cartesian marker positions, human base link position and orientation[11] and local Cartesian position of the makers with respect to the base link are computed via (1), (2) and (3). Each motion primitive consists of the three-dimensional base link position, the four-dimensional base link quaternion, and 60 elements for the position vectors of the 20 markers on the upper body shown in Figure 12.

From the human motion data set, 11 HMMs are trained via the off-line EM algorithm: *Dual-Arm Circle* motion, *Leaning Backward* motion, *Forward Bow* motion, *Bye-Bye* motion, *Leaning Left* motion, *Left Hand Up&Down* motion, *Squat* motion, *Right Hand Punch* motion, *Dual-Arm 3-Beat Conducting* motion, *Right Hand Up&Down* motion, *Leaning Right* motion. Each HMM is trained from five exemplars and consists of 20 states. The structure of HMMs (e.g. the number of states) is simply chosen from experimental experiences. However, rough estimation of structure is enough without sensitive manual tuning. From our experiences, HMMs with 15–20 states work well with whole body motion patterns. For a discussion of the model selection problem for HMMs, refer to Billard et al. (2006), Dixon et al. (2004), and Kulić et al. (2007a). Also, a factorial HMM-based methodology (Kulić et al. 2007b; Lee et al. 2008a) can avoid over-fitting problems with large numbers of states and poor generation and discrimination performance with small numbers of states, which are encountered with HMMs.

The human performs several motions in a random order. While the humanoid is controlled directly by markers, a series of different human motions are recognized successively online. Table 1 shows the log-likelihood to generate observed motions (*Dual-Arm Circle*, *Left Hand Up&Down*, and *Bye-Bye* motion) from each HMM. From the table, one can see that all observed motions are well recognized since the corresponding HMMs have the highest likelihood. More specifically, the *Bye-Bye* HMM has the highest log-likelihood for a *Bye-Bye* motion pattern. Online motion recognition was performed with a sampling rate of about 15 ms.

Each motion primitive is generated using a Monte Carlo method of generation from the associated HMM. Figures 17 and 18 show the generated motion primitive of a *Leaning Backward* motion and a *Leaning Left* motion from the associated HMMs. The figures show that the characteristics of the motion primitives are well preserved. From the experiments in this section, one can see that the learned motion primitives are used easily for recognition of the humans's motion and generation of the humanoid's motion. After

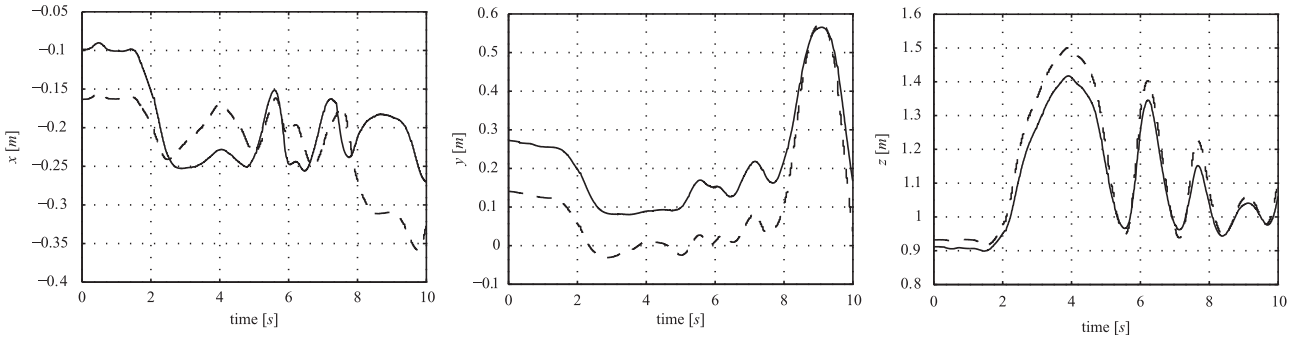


**Fig. 16.** Position of marker 2 on the right wrist. The dashed line shows the measured marker position on the human, and the solid line shows the motion of the corresponding point of the robot.

**Table 1.** Recognition Results of Human Motions. Log-likelihood for Three Observations.

| HMM name | *Dual-Arm Circle* | *Left Hand Up&Down* | *Bye-Bye* |
|---|---|---|---|
| *Dual-Arm Circle* | **−71.96** | 82.54 | −23.78 |
| *Leaning Backward* | −349.78 | 6.14 | −118.58 |
| *Forward Bow* | −358.74 | −6.90 | −100.47 |
| *Bye-Bye* | −330.55 | −312.99 | **190.46** |
| *Leaning Left* | −406.76 | 27.77 | −155.35 |
| *Left Hand Up&Down* | −317.56 | **156.02** | −132.53 |
| *Squat* | −413.37 | −33.29 | −141.41 |
| *Right Hand Punch* | −162.02 | 61.41 | −160.44 |
| *Dual-Arm 3 Beat Conducting* | −123.90 | 106.17 | −48.83 |
| *Right Hand Up&Down* | −263.68 | −52.18 | 64.28 |
| *Leaning Right* | −132.70 | 83.00 | 8.87 |

motion primitive learning, the self-motions can be reproduced anytime without the help of a human expert.

## 6.3. Evaluation of Impedance Control

In this section, the force response of the impedance controller from Section 5.1 is exemplified by the humanoid's left elbow joint. A human user "smoothly" exerted external forces at the robot's end-effector. Based on the Jacobian matrix, these forces are transformed into the external joint torques $\tau_{ext}$ for the implementation of (6). For the evaluation, we performed a comparison of the non-linear stiffness term (7) with a simple linear spring with constant stiffness $s_0 = 100\,\mathrm{Nm\,rad^{-1}}$. The joint-level inertia for the elbow joint was chosen as $M_I = 1\,\mathrm{Nms^2\,rad^{-1}}$. For the case of (7), the maximum torque was set to $\tau_{max} = 10\mathrm{Nm}$. The measurement results are shown in Figure 19. Therein, one can see that the behavior for small deviations $\Delta q$ is quite similar, but for larger deviations the contact torque of the impedance with (7) remains bounded. Note that $\tau_{max}$ is not a "hard bound" for the real contact torque, but rather limits the stiffness term in the impedance. For dynamic motions, larger torques can result due to the influence of inertia and damping, as well as due to the dynamics of the underlying position controller. Also, one can see that the damping of the impedance for larger deviations is low, since the damping term (8) is computed based on the local derivative $\partial\tau_k(\Delta q)/\partial\Delta q$.

## 6.4. Evaluation of Mimetic Communication

Please note that a supervised learning approach is used in the present paper. Therefore, a training data set is segmented and labeled manually by a supervisor. Twelve motion primitives and eight interaction primitives are trained. The 12 motion primitives are *Home Positioning*, *High Ten*, *Right Hand High Five*, *Left Hand High Five*, *Low Ten Request*, *Low Ten Answer*, *Right Hand Low Five Request*, *Right Hand Low Five Answer*, *Right Hand Low Five Request*, *Right Hand Low Five Answer*, *Fist Hitting Request*, and *Fist Hitting Answer* motion. The eight interactions are *Home Positioning*, *High Ten*, *Right Hand High Five*, *Left Hand High Five*, *Low Ten*, *Right Hand Low Five*, *Right Hand Low Five*, and *Fist Hitting* interaction. Periodic continuous HMMs are used for motion primitives and left-to-right discrete HMMs are used for interaction primitives.

A human performs several motions in a random order. A series of different human motions are recognized and an appropriate interaction strategy is found successively online. Snapshots during physical interaction between the human and the robot are shown in Figure 24. The recognition performance is tested during a 17-minute-long

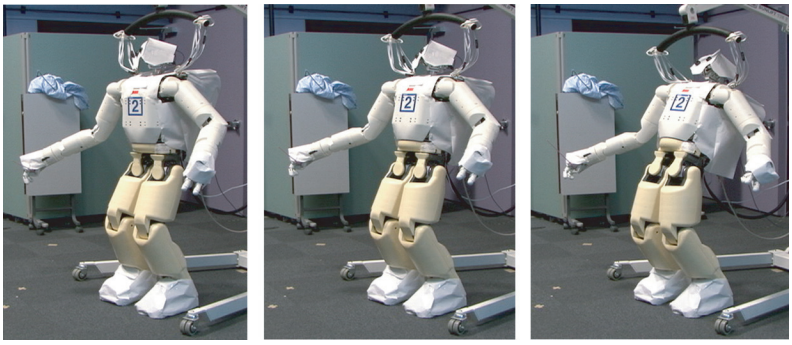

**Fig. 17.** *Leaning Backward* motion, generated from the corresponding HMM (see Extension 1).

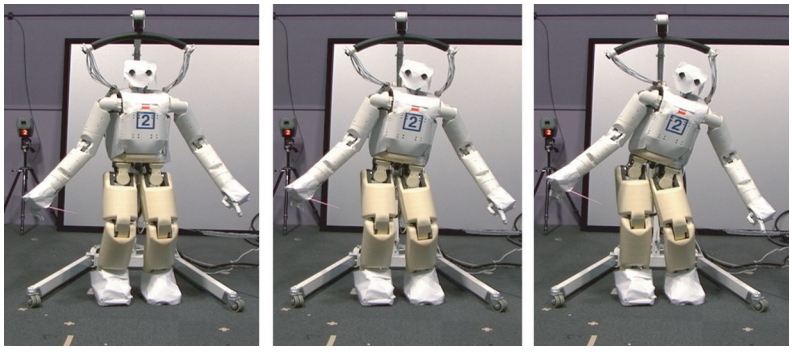

**Fig. 18.** *Leaning Left* motion, generated from the corresponding HMM (see Extension 1).

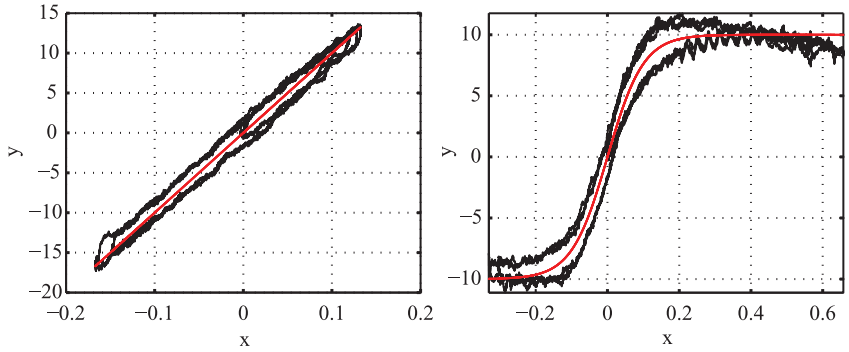


**Fig. 19.** Evaluation of the impedance controller for the humanoid's elbow joint. The left plot shows an implementation of the impedance (6) with a linear spring with constant stiffness $s_0 = 100\text{Nmrad}^{-1}$ instead of (7). The right plot shows the result with the non-linear stiffness term (7) for the case $\tau_{\max} = 10\text{Nm}$. The thin line shows the static characteristic curve of the stiffness term only, i.e. without the influence of inertia and damping.

experiment. During the experiment, there were 134 interactions in total and 4 failure cases occurred giving a success ratio of 97% for the interaction primitives recognition[12]. Since interaction primitive recognition is based on the result of motion primitive recognition, the success ratio for motion primitive recognition is higher than 97%. Among the four failure cases of interaction primitive recognition, two cases were caused by wrong recognition of motion primitives. In the other two cases, the human demonstrator smoothly connected two successive interaction patterns by skipping the *Home Positioning* motion primitive. Therefore, the *Home Positioning* motion primitive was not detected. Since such short-cut connections were not observed during the training procedure, correct interaction primitives were not recognized. However, this is not a fundamental limitation of the proposed method. This can be interpreted as that the robot can recognize the learned motion primitives, however the robot has difficulties to recognize completely unknown patterns. To put it simply, if a long natural

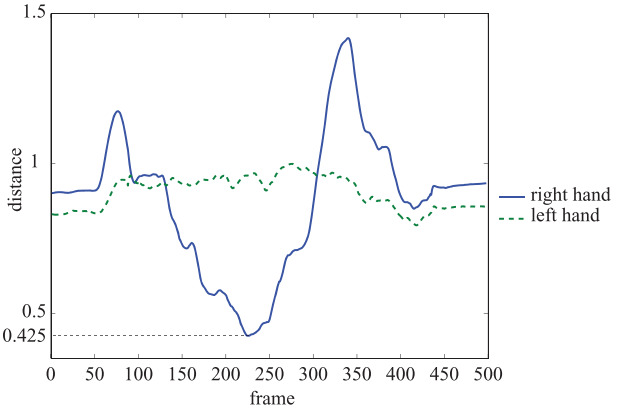


**Fig. 20.** Distances between robot hands and corresponding human hands during *Right Hand High Five* motion, when simply following generated motion trajectory from the motion primitive. The shortest distance between robot and human hands is 0.425 m and thus no physical contact occurred.

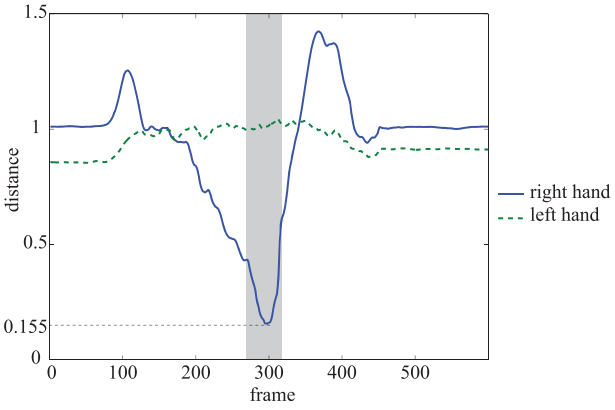


**Fig. 22.** Distances between robot hands and corresponding human hands, when a spring between the robot and human hands is activated during *Right Hand High Five* motion. By using the real-time motion adaptation strategy, physical contact is established.

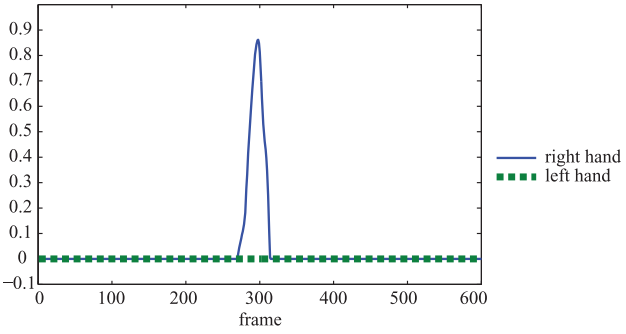


**Fig. 21.** The $\delta$ value of the hand spring during *Right Hand High Five* motion. Then $\delta$ value is changed by the expected distance between the robot and human hands.

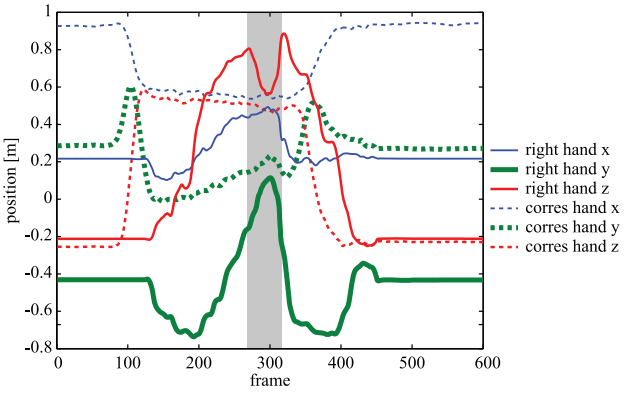


**Fig. 23.** Robot right hand position and its corresponding human hand, when a spring between the robot and human hands is activated during right hand high five motion.

motion sequence which includes short-cut connections is used for training data, such short-cut connections can be recognized correctly. Note that this does not mean that a human supervisor has to teach a robot every single motion pattern. Since a motion primitive is represented in a probabilistic way in our method, it can cover a variety of similar motion patterns. The good generality of a stochastic modeling (e.g. HMMs) has been shown in many recent works (Kulić et al. 2008; Lee et al. 2008b; Calinon et al. 2009). Specifically saying, a motion primitive which is learned from a few demonstrations was used for recognition and generation of a variety of similar motion patterns. Note also that, although our proposed method can handle some portion of missing markers and wrong marker labeling, when marker labeling is totally wrong, the system might become erratic.

The mimetic communication strategy described in Section 4 allows human motion patterns to be recognized, appropriate interaction patterns to be found, and robot motion patterns to be generated. However, simply following the generated marker trajectories from HMMs cannot achieve the realistic interaction. Figure 20 illustrates the distance between corresponding hands of the robot and human, when simply following the generated marker trajectories from the *Right Hand High Five* motion primitive without the real-time motion adaptation strategy in Section 5.2. The solid line is the distance between robot's right hand and the corresponding human's right hand. The dotted line shows results for the left hand. The closest distance between robot and human hands is 0.425 m and thus no physical contact occurred.

On the other hand, by using the motion adaptation strategy in Section 5.2, clear human–robot contacts were made (Figures 21–23). Figure 21 illustrates the trajectories of the weighting parameters $\delta_r$ and $\delta_l$ of the spring between human's and robot's hands. Around frame 300, the weighting parameter of the spring of the right hand is increased which means that the robot right hand is pulled to the real human right hand by the virtual spring (the large bold spring in Figure 11) to achieve physical contact.

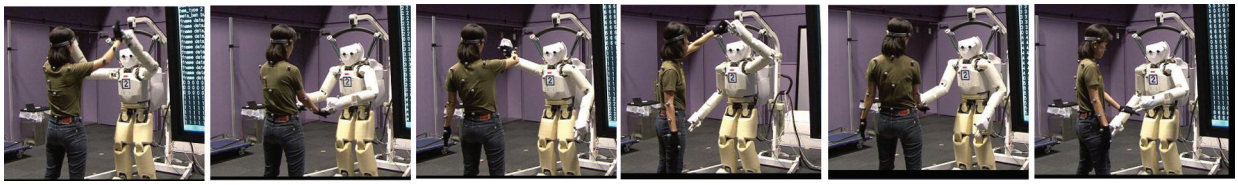

**Fig. 24.** Physical human–robot interaction using the mimetic communication model in the experiments (see Extension 1).

Figure 22 illustrates the real distance between the corresponding hands. By comparing Figure 20 and Figure 22, one can see that the closest distance between the robot's right hand and the corresponding human's hand is decreased from 0.425 to 0.155 m by using the real-time motion adaptation strategy. This distance is measured using markers on the human's and robot's wrist. A distance of this magnitude means that the fingers were already in contact. The gray colored region shows the time period when the hand spring was activated (i.e. at the time in which the weighting parameter of the right hand spring was not zero in Figure 21).

Figure 23 shows the trajectories of the robot's (solid lines) and human's right hand (dotted lines). During the time when the spring between the robot's and human's hand was activated (gray colored region), the robot's hand position is close to the human's hand position. In particular, as can be seen from the robot's hand $z$ trajectory (height), the robot's hand was higher than the human's hand before the gray region. Within the gray region the robot's hand goes down to the human's hand to establish contact. Afterwards, it returns to the reference trajectory generated from the motion primitive. Owing to the gradual activation of the hand spring via the $\delta$ value and the computation of the desired trajectory via the simulation of the upper body dynamics, the motion primitive is adapted in a smooth way.

## 7. Conclusion

In this paper we have proposed a mimetic communication method in which a humanoid robot interacts with a human by behaviors including physical contacts. The humanoid robot imitates the human's motion pattern by a direct marker control method in Cartesian space. With the baseline of simple motion imitation, the robot learns motion primitives and interaction primitives in an imitative learning way because of its efficiency and intuitiveness. During the interaction primitive learning procedure, the robot is involved actively by using previously acquired motion primitives and measuring additional sensory information such as physical contacts. The interaction primitives encode the causality of motions (one agent's action and the other agent's reaction), contact information (e.g. when and where contacts occur). Through the concept of the imitation primitives and interaction primitives, the mimetic communication model recognizes the human's motion, selects the interaction strategy, and commands the reference trajectory and expected contact information to the robot. The reference trajectory is executed by means of the direct marker control. According to the expected contact information, the reference trajectory is reshaped for the adaptation to the human's motions in real-time. For performing safe contacts, an impedance controller is integrated into the setting. All of the presented concepts were evaluated in experiments with a human-size humanoid robot, as shown in Extension 1 attached to the paper.

The main contributions are summarized as follows.

1. A motion imitation method via "marker control" is proposed. By implementing virtual springs between a human and a humanoid robot, the robot can imitate the target motions in task space without the need of computing inverse kinematics. In combination with the simulation of the upper body dynamics, motion imitation and motion learning becomes robust with respect to missing markers.
2. Behavioral communication in symbolic and physical domains are combined. The communication in the symbolic domain is realized through the concept of motion primitives and interaction primitives. In the physical domain, the trajectory of the motion primitive is reshaped in accordance with the dynamic environment (e.g. changes of the human's hand motion) in real-time. Motion adaptation is realized by tightly connecting learned primitives and controllers.
3. Key strategies of our learning method are "imitation of a human" and "active involvement". This is an intuitive and efficient learning scheme. The robot's active involvement provides important sensory information in the physical domain and supports incremental learning by actively reusing the previously acquired knowledge.
4. To the best of our knowledge, this is the first work which extends imitation learning to a *physical* HRI task including compliant contact and an active involvement of the robot in the learning.

**Acknowledgment**

The authors would like to thank Wataru Takano for his valuable discussion and Akihiko Murai for his supports in the operation of the motion capture system. This research is partly supported by Special Coordination Funds for Promoting Science and Technology, "IRT Foundation to Support Man and Aging Society".

## Notes

1. Readers not familiar with the concept of SE(3) may consider it as the space of homogeneous matrices, i.e. $\mathbb{R}^{3\times4}$ in which the left three-by-three matrix is a rotation matrix. Similarly, se(3) and se$^*$(3) can be taken as $\mathbb{R}^6$ and describe six-dimensional generalized velocities and forces. The use of SE(3) instead of using local coordinates in (1) allows us to avoid the singularity problem of minimal representations of the base orientation.
2. Equation (1) represents the integration of the base link position and orientation via the body twist. The symbol $\tilde{\xi} \in \mathbb{R}^{4\times4}$ is defined as $\tilde{\xi} = [S, v; 0]$ with $S \in \mathbb{R}^{3\times3}$ as the skew symmetric matrix computed from the rotational component of and $\xi$ and $v \in \mathbb{R}^3$ as the translational component (Murray et al. 1994).
3. In this paper, a "motion primitive" denotes a probabilistic representation of a motion type. In other words, one motion primitive covers not only one specific motion pattern but a larger set of similar motion patterns. In a similar way, but on a higher level of abstraction, we model the continuous interaction between humans as sequences of elementary atomic interaction segments, which we call interaction primitives.
4. While one could in principle use CHMMs also in the upper level (interaction primitives), we think that a discrete model is a more intuitive representation for the rule-based interactions. On the lower level (motion primitives), the continuous CHMMs are used for the description of the human's and robot's motions due to the continuous nature of motion signals.
5. In order to recognize complicated interaction patterns, not only the human behavior but also the robot behavior should be considered.
6. The details of the proto-symbol space construction method can be found in Inamura et al. (2003).
7. See Eggert et al. (1997) for a comparison of four similar algorithms of rigid-body pose estimation.
8. Motion patterns are decoded using the expectation operator in the stochastic model. The motion generation is a two-stage stochastic process: state transition generation and motion output generation from the state transition. See Lee and Nakamura (2010) for the further details.
9. One reason for partial input data simply is that the hand correspondence is not known *a priori*. Moreover, simple interactions can be recognized by observing the human's behavior only. For complicated interaction recognition, the robot's behavior is also necessary.
10. This is $\tanh(x) = (\exp(x) - \exp(-x))/(\exp(x) + \exp(-x))$.
11. To be precise, the base link motion relative to its initial pose is transmitted to the mimesis algorithm.
12. From the video record of the experiment, a human counted how many interactions occurred during the experiment. The person also counted how many recognition failures happened. Herein, the recognition failure denotes that the robot recognized a different primitive to the person.

## References


Albu-Schäffer, A., Eiberger, O., Grebenstein, M., Haddadin, S., Ch. Ott, Wimboeck, T., Wolf, S., and Hirzinger, G. (2008). Soft robotics: From torque feedback controlled lightweight robots to intrinsically compliant systems. *Robotics and Automation Magazine*, **15**(3): 20–30.

Albu-Schäffer, A., Ott, Ch., Frese, U., and Hirzinger, G. (2003). Cartesian impedance control of redundant robots: Recent results with the DLR-light-weight-arms. *IEEE International Conference on Robotics and Automation*, 3704–3709.

Arnold, V. (1989). *Mathematical Methods of Classical Mechanics*, 2nd edition. Berlin, Springer.

Asfour, T., Gyarfas, F., Azad, P., and Dillmann, R. (2006). Imitation learning of dual-arm manipulation tasks in humanoid robots. *IEEE-RAS International Conference on Humanoid Robots*, pp. 40–47.

Bicchi, A. and Tonietti, G. (2004). Dealing with the safety-performance tradeoff in robot arm design and control: fast and "soft-arm" tactics. *IEEE Robotics and Automation Magazine*, pp. 22–33.

Billard, A., Calinon, S., Dillmann, R., and Schaal, S. (2008). *Robot Programming by Demonstration* (*Handbook of Robotics*), Siciliano, B. and Khatib, O. (eds.). Berlin, Springer.

Billard, A., Calinon, S., and Guenter, F. (2006). Discriminative and adaptive imitation in uni-manual and bi-manual tasks. *Robotics and Autonomous Systems*, **54**: 370–384.

Billard, A. and Dautenhahn, K. (1998). Grounding communication in autonomwous robots: experimetnal study. *Robotics and Autonomous Systems*, **24**: 71–79.

Billard, A. and Hayes, G. (1998). Drama, a connectionist architecture for control and learning in autonomous robots. *Adaptive Behaviour Journal*, **7**(2): 35–64.

Breazeal, C. and Scassellati, B. (2002). Robots that imitate humans. *Trends in Cognitive Science*, **6**(11): 481–487.

Calinon, S. and Billard, A. (2007). Active teaching in robot programming by demonstration. *IEEE International Conference on Robot and Human Interactive Communication*, pp. 702–707.

Calinon, S. and Billard, A. (2008). A probabilistic programming by demonstration framework handling constraints in joint space and task space. *IEEE/RSJ International Conference on Intelligent Robots and Systems*, pp. 367–372.

Calinon, S., Evrard, P., Gribovskaya, E., Billard, A., and Kheddar, A. (2009). Learning collaborative manipulation tasks by demonstration using a haptic interface. *IEEE International Conference of Advanced Robotics*.

Cheng, G., Hyon, S.-H., Morimoto, J., Ude, A., Colvin, G., Scroggin, W., and Jacobsen, S. C. (2006). CB: a humanoid research platform for exploring neuroscience. *IEEE-RAS International Conference on Humanoid Robots*.

Cox, M. and Cox, M. (2001). *Multidimensional Scaling*. London, Chapman and Hall.

Dariush, B., Gienger, M., Jian, B., Goerick, C., and Fujimura, K. (2008). Whole body humanoid control from human motion descriptors. *IEEE International Conference on Robotics and Automation*, pp. 2677–2684.

Demircan, E., Sentis, L., Sapio, V. D., and Khatib, O. (2008). Human motion reconstruction by direct control of marker trajectories. *Advances in Robot Kinematics (ARK)*.

Dempster, A., Laird, N., and Rubin, D. (1977). Maximum likelihood from incomplete data via the EM algorithm. *Journal of the Royal Statistical Society*, **39**(1): 1–38.

Dillmann, R. (2004). Teaching and learning of robot tasks via observation of human performance. *Robotics and Autonomous Systems*, **47**: 109–116.

Dixon, K. R., Dolan, J. M., and Khosla, P. K. (2004). Predictive robot programming: theoretical and experimental analysis. *The International Journal of Robotics Research*, **23**: 955–973.

Donald, M. (1991). *Origins of the Modern Mind*. Cambridge, MA, Harvard University Press.

Eggert, D. W., Lorusso, A., and Fisher, R. B. (1997). Estimating 3-d rigid body transformations: a comparison of four major algorithms. *Machine Vision and Applications*, **9**: 272–290.

Fod, A., Matarić, M., and Jenkins, O. (2002). Automated derivation of primitives for movement classification. *Autonomous Robots*, **12**(1): 39–54.

Gallese, V., Fadiga, L., Fogassi, L., and Rizzolatti, G. (1996). Action recognition in the premotor cortex. *Brain*, **119**: 593–609.

Harville, D. (1997). *Matrix Algebra from a Statistician's Perspective*. Berlin, Springer.

Hirzinger, G., Sporer, N., Albu-Schäffer, A., Hähnle, M., Krenn, R., Pascucci, A., and Schedl, M. (2002). DLR's torque-controlled light weight robot III–-are we reaching the technological limits now? *IEEE International Conference on Robotics and Automation*, pp. 1710–1716.

Hogan, N. (1985). Impedance control: an approach to manipulation, part I–theory. *ASME Journal of Dynamic Systems, Measurement, and Control*, **107**: 1–7.

Horn, B. K. P. (1987). Closed-form solution of absolute orientation using unit quaternions. *Journal of the Optical Society of America*, **4**: 629–642.

Hunt, K. and Crossley, F. (1975). Coefficient of restitution interpreted as damping in vibroimpact. *Transactions of the ASME: Journal of Applied Mechanics*, **42**: 440–445.

Ijspeert, A. J., Nakanishi, J., and Schaal, S. (2002). Movement imitation with nonlinear dynamical systems in humanoid robots. *IEEE International Conference on Robotics and Automation*, pp. 1398–1403.

Inamura, T., Nakamura, Y., and Toshima, I. (2004). Embodied symbol emergence based on mimesis theory. *The International Journal of Robotics Research*, **23**(4): 363–377.

Inamura, T., Tanie, H., and Nakamura, Y. (2003). From stochastic motion generation and recognition to geometric symbol development and manipulation. *IEEE-RSJ International Conference on Humanoid Robots*, 1b–02.

Janus, B. and Nakamura, Y. (2005). Unsupervised probabilistic segmentation of motion data for mimesis modeling. *the 12th IEEE International Conference on Advanced Robotics*, pp. 411–417.

Kanehiro, F., Suleiman, W., Lamiraux, F., Yoshida, E., and Laumond, J.-P. (2008). Integrating dynamics into motion planning for humanoid robots. *IEEE/RSJ International Conference on Intelligent Robots and Systems*, pp. 660–667.

Khatib, O. (1987). A unified approach for motion and force control of robot manipulators: the operational space formulation. *IEEE Journal of Robotics and Automation*, **3**(1): 1115–1120.

Kosuge, K. and Hirata, Y. (2004). Human–robot interaction. *IEEE International Conference on Robotics and Biomimetics*, pp. 8–11.

Kuffner, J., Nishiwaki, K., Kagami, S., Inaba, M., and Inoue, H. (2001). Motion planning for humanoid robots under obstacle and dynamic balance constraints. *IEEE International Conference on Robotics and Automation*, pp. 692–698.

Kulić, D., Takano, W., and Nakamura, Y. (2007a). Incremental on-line hierarchical clustering of whole body motion patterns. *IEEE International Symposium on Robot and Human Interactive Communication*.

Kulić, D., Takano, W., and Nakamura, Y. (2007b). Representability of human motions by factorial hidden Markov models. *IEEE/RSJ International Conference on Intelligent Robots and Systems*.

Kulić, D., Takano, W., and Nakamura, Y. (2008). Combining automated on-line segmentation and incremental clustering for whole body motions. *IEEE International Conference on Robotics and Automation*, pp. 2591–2598.

Kunori, H., Lee, D., and Nakamura, Y. (2009). Associating and reshaping of whole body motions for object manipulation. *IEEE/RSJ International Conference on Intelligent Robots and Systems*, pp. 5240–5247.

Lee, D., Kulić, D., and Nakamura, Y. (2008a). Missing motion data recovery using factorial hidden markov models. *IEEE International Conference on Robotics and Automation*, pp. 1722–1728.

Lee, D., Kunori, H., and Nakamura, Y. (2008b). Association of whole body motion from tool knowledge for humanoid robots. *IEEE/RSJ International Conference on Intelligent Robots and Systems*, pp. 2867–2874.

Lee, D. and Nakamura, Y. (2005). Mimesis from partial observations. *IEEE/RSJ International Conference on Intelligent Robots and Systems*, pp. 1911–1916.

Lee, D. and Nakamura, Y. (2010). Mimesis model from partial observations for a humanoid robot. *The International Journal of Robotics Research*, **29**(1): 60–80.

Lee, D., Ott, C., and Nakamura, Y. (2009). Mimetic communication with impedance control for physical human–robot interaction. *IEEE International Conference on Robotics and Automation*, pp. 1535–1542.

Marhefka, D. W. and Orin, D. E. (1999). A compliant contact model with nonlinear damping for simulation of robotic systems. *IEEE Transactions on Systems, Man, and Cybernetics-Part A: Systems and Humans*, **29**(6): 565–572.

Murray, R., Li, Z., and Sastry, S. (1994). *A Mathematical Introduction to Robotic Manipulation*. Boca Raton, FL, CRC Press.

Nagai, Y., Hosoda, K., Morita, A., and Asada, M. (2003). A constructive model for the development of joint attention. *Connection Science*, **15**(4): 211–229.

Nakamura, Y., Takano, W., and Yamane, K. (2005). Mimetic communication theory for humanoid robots interacting with humans. *International Symposium of Robotics Research*, pp. 12–15.

Nakamura, Y. and Yamane, K. (2000). Dynamics computation of structure-varying kinematic chains and its application to human figures. *IEEE Transactions on Robotics*, **16**(2): 124–134.

Nakaoka, S., Nakazawa, A., Kanahiro, F., Kaneko, K., Morisawa, M., and Ikeuchi, K. (2005). Task model of lower body motion for a biped humanoid robot to imitate human dances. *IEEE/RSJ International Conference on Intelligent Robots and Systems*, pp. 2769–2774.

Okada, M., Tatani, K., and Nakamura, Y. (2002). Polynomial design of the nonlinear dynamics for the brain-like information processing of whole body motion. *IEEE International Conference on Robotics and Automation*, pp. 1410–1415.

Ott, C., Lee, D., and Nakamura, Y. (2008). Motion capture based human motion recognition and imitation by direct marker control. *IEEE-RAS International Conference on Humanoid Robots*, pp. 399–405.

Ott, Ch., Eiberger, O., Friedl, W., Bäuml, B., Hillenbrand, U., Borst, Ch., Albu-Schäffer, A., Brunner, B., Hirschmüller, H., Kielhöfer, S., Konietschke, R., Suppa, M., Wimböck, T., Zacharias, F., and Hirzinger, G. (2006). A humanoid two-arm system for dexterous manipulation. *IEEE-RAS International Conference on Humanoid Robots*, pp. 276–283.

Peters, J., Vijayakumar, S., and Schaal, S. (2003). Reinforcement Learning for Humanoid Robotics.

Pollard, N., Hodgins, J., Riley, M., and Atkeson, C. (2002). Adapting human motion for the control of a humanoid robot. *IEEE International Conference on Robotics and Automation*, pp. 1390–1397.

Rabiner, L. R. (1989). A tutorial on hidden Markov models and selected applications in speech recognition. *Proceedings IEEE*, **77**(2): 257–286.

Rizzolatti, G. and Arbib, M. (1998). Language within our grasp. *Trend in Neurosciences*, **21**: 151–152.

Rizzolatti, G. and Craighero, L. (2004). The mirror-neuron system. *Annual Reviews of Neuroscience*, **27**: 169–192.

Rizzolatti, G., Fadiga, L., Gallese, V., and Fogassi, L. (1996). Premotor cortex and the recognition of motor actions. *Cognitive Brain Research*, **3**: 131–141.

Santis, A. D., Siciliano, B., Luca, A. D., and Bicchi, A. (2008). An atlas of physical humanrobot interaction. *Mechanism and Machine Theory*, **43**(3): 253270.

Schaal, S. (1999). Is imitation learning the route to humanoid robots? *Trends in Cognitive Sciences*, **3**(6): 233–242.

Schaal, S., Ijspeert, A., and Billard, A. (2003). Computational approaches to motor learning by imitation. *Philosophical Transaction of the Royal Society of London: Series B, Biological Sciences*, **358**: 537–547.

Shibata, T., Tashima, T., and Tanie, K. (1999). Emergence of emotional behavior through physical interaction between human and robot. *IEEE International Conference on Robotics and Automation*, pp. 2868–2873.

Sumioka, H., Yoshikawa, Y., and Asada, M. (2008). Learning of joint attention from detecting causality based on transfer entropy. *Journal of Robotics and Mechatronics*, **20**(3): 378–385.

Takano, W. and Nakamura, Y. (2006). Humanoid robot's autonomous acquisition of proto-symbols through motion segmentation. *IEEE-RAS International Conference on Humanoid Robots*, pp. 425–431.

Takano, W., Yamane, K., Sugihara, T., Yamamoto, K., and Nakamura, Y. (2006). Primitive communication based on motion recognition and generation with hierarchical mimesis model. *IEEE International Conference on Robotics and Automation*, pp. 3602–3609.

Tani, J. and Ito, M. (2003). Self-organization of behavioral primitives as multiple attractor dynamics: a robot experiment. *IEEE Transactions on Systems, Man, and Cybernetics. Part A: Systems and Humans*, **33**(4): 481–488.

Zinn, M., Khatib, O., Roth, B., and Salisbury, J. (2004). A new actuation concept for human-friendly robot design: Playing it safe. *IEEE Robotics and Automation Magazine*, pp. 12–21.

## Appendix: Index to Multimedia Extensions

The multimedia extension page is found at http://www.ijrr.org

Table of Multimedia Extensions

| Extension | Type | Description |
|---|---|---|
| 1 | Video | Human motion imitation and "high five" interaction implemented with the IRT humanoid robot |